Structure of the Cytoplasmic Domain of Erythrocyte Band 3 Hereditary Spherocytosis Variant P327R: Band 3 Tuscaloosa†

Zheng Zhou,‡ Susan C. DeSensi,§ Richard A. Stein,‡ Suzanne Brandon,‡ Likai Song,|| Charles E. Cobb,‡ Eric J. Hustedt,‡ and Albert H. Beth‡*

Molecular Physiology and Biophysics and Center for Structural Biology, Vanderbilt University, Nashville, Tennessee 37232, and Institute of Molecular Biophysics, The National High Magnetic Field Laboratory, Department of Biological Sciences, Florida State University, Tallahassee, Florida 32310

Received May 17, 2007; Revised Manuscript Received July 10, 2007

ABSTRACT: Previous studies have shown that a single P327R point mutation in the cytoplasmic domain of band 3 (cdb3) protein, known as band 3 Tuscaloosa, leads to a reduction in protein 4.2 content of the erythrocyte membrane and hemolytic anemia. Recent studies have shown that this point mutation does not dissociate the cdb3 dimer, nor does it lead to large-scale rearrangement of the protein structure (Bustos, S. P., and Reithmeier, R. A. F. (2006) *Biochemistry 45*, 1026−1034). To better define the structural changes in cdb3 that lead to the hemolytic anemia phenotype, site-directed spin labeling (SDSL), in combination with continuous wave electron paramagnetic resonance (EPR) and pulsed double electron−electron resonance (DEER) spectroscopies, has been employed in this study to compare the structure of the R327 variant with wild type P327 cdb3. It is confirmed that the P327R mutation does not dissociate the cdb3 dimer, nor does it change the spatial orientation of the two peripheral domains relative to the dimer interface. However, it does affect the packing of the C-terminal end of helix 10 of the dimerization arms in a subpopulation of cdb3 dimers, it leads to spectral changes at some residues in β-strand 11 and in the N-terminal end of helix10, and it produces measurable spectral changes at other residues that are near the mutation site. The data indicate that the structural changes are subtle and are localized to one surface of the cdb3 dimer. The spectroscopic description of structural features of the P327R variant provides important clues about the location of one potential protein 4.2 binding surface on cdb3 as well as new insight into the structural basis of the membrane destabilization.

In the resting state, human erythrocytes exhibit a biconcave disk shape. During blood flow through the peripheral circulation, erythrocytes must deform in order to traverse the systemic capillaries (*1*). The membrane skeleton network provides erythrocytes with the mechanical stability, deformability, and elasticity to survive in circulation. Many alterations in the composition and arrangement of the membrane skeleton proteins cause hereditary hemolytic anemia (reviewed in ref *2*). Generally, defects in the "horizontal" interactions of membrane skeleton components, such as loss of spectrin heterodimer/heterotetramer associations (*3*) and deficiency of protein 4.1 (*4*−*6*), result in hereditary elliptocytosis (HE) and hereditary pyropoikilocytosis (HPP). Defects in the "vertical" interactions of membrane skeleton components, such as an abnormal band 3−ankyrin−spectrin junction (*7*, *8*), are often associated with hereditary spherocytosis (HS)[1] (*9*, *10*).

The incidence of HS is one family of 2000−3000. Among Caucasians, approximately 15−20% of HS cases result from band 3 defects (*8*). In these HS patients, erythrocytes adopt different degrees of spherical shape with decreased cell size instead of the normal biconcave disk shape. These spherical erythrocytes are more osmotically fragile and less deformable than normal cells (*7*, *11*). Mutations causing HS have been mapped to genes SPTA1, SPTB, ANK1, EPB42 and SLC4A1, encoding spectrin α-chain, spectrin β-chain, ankyrin, protein 4.2, and anion exchanger 1 (AE1, also known as band 3), respectively (*8*).

Band 3 is the most abundant integral membrane protein in human erythrocytes (*12*). It is composed of two structurally and functionally distinct domains (*13*−*15*). The C-terminal transmembrane domain forms an anion exchanger that facilitates the exchange of bicarbonate and chloride anions across the membrane (*11*, *16*, *17*). The N-terminal cytoplasmic domain of band 3 (cdb3) functions as an anchoring

† This work was supported by Grants R37 HL034737 and S10 RR019120 (A.H.B.) from the National Institutes of Health. The EPR instrumentation at the National High Magnetic Field Laboratory was purchased on Grant CHE-0079649 from the National Science Foundation, and predoctoral support was provided by the American Heart Association (L.S.).

* Corresponding author [telephone (615) 322-4235; fax (615) 322-7236; e-mail al.beth@vanderbilt.edu].

‡ Molecular Physiology and Biophysics, Vanderbilt University.

§ Center for Structural Biology, Vanderbilt University.

|| Florida State University.

[1] Abbreviations: AE1, anion exchanger 1; CD, circular dichroism; cdb3, cytoplasmic domain of band 3; cw, continuous wave; DEER, double electron−electron resonance; ELDOR, electron−electron double resonance; EPR, electron paramagnetic resonance; HS, hereditary spherocytosis; MTSSL, 1-oxyl-2,2,5,5-tetramethyl-Δ3-pyrroline-3-methyl methanethiosulfonate spin label; NiEDDA, nickel(II) ethylenediaminediacetate; PBS, phosphate-buffered saline; SDSL, site-directed spin labeling; SDS-PAGE, sodium dodecyl sulfate−polyacrylamide gel electrophoresis; T_{1e}, electron spin−lattice relaxation time; TPX, trademark for polymethylpentene.

10.1021/bi700948p CCC: $37.00
Published on Web 08/16/2007

component for other peripheral membrane-associated proteins (*18*). The protein complex of cdb3, ankyrin (*19*), protein 4.2 (*19*, *20*), and protein 4.1 (*21*) together with the spectrin−actin membrane skeleton network plays an important role in maintaining erythrocyte shape and mechanical stability (*22*−*24*) and providing flexibility and elasticity (*25*, *26*).

A considerable number of band 3 mutations (more than 40) associated with HS have been identified and sequenced including missense mutations, nonsense mutations, frameshifts, insertions, and deletions. Most of these are sporadic mutations and dominantly inherited (*8*, *11*, *27*). Among these mutations, band 3 Tuscaloosa (P327R) is very interesting. The clinical phenotype of P327R is atypical HS with moderate hemolytic anemia. The erythrocyte membrane has a partial (29 ± 5%) deficiency of protein 4.2. The binding of ankyrin to inside-out vesicles (IOVs) prepared from peripheral venous blood is in the normal range. In contrast, the predicted maximal binding capacity of these IOVs for protein 4.2 decreases 20−33% (*28*).

The crystal structure of wt-cdb3 (residues 55−356) has been determined at pH 4.8 (*29*). Previous work has shown that the structure determined at this low pH agrees very well with the structure in solution at pH 7 as revealed by site-directed spin-labeling (SDSL) studies (*30*). The cdb3 structure at atomic resolution greatly facilitates localization of HS-causing mutations, which have normal expression levels but abnormal function (*31*). Proline 327 is located in the loop region on the highly conserved dimerization arm (304−357) (*29*). Recent studies on the P327R mutation indicated that isolated cdb3 maintained its overall protein fold and dimeric state, but exhibited slightly reduced thermal stability (*32*−*34*). To better understand this alteration in stability and the structural basis for the HS phenotype, SDSL studies have been carried out in this work. Experiments combining conventional cw-EPR and pulsed-double electron−electron resonance (DEER) were conducted on selected single cysteine cdb3 proteins with the P327R mutation. The data from these studies confirm that substitution of arginine for proline 327 subtly destabilizes cdb3 as reflected in a moderate decrease in melting temperature without inducing dimer dissociation. No global structural changes in the peripheral domains of the cdb3 dimer or in their spatial arrangement were detected. Structural disturbances caused by the P327R mutation localize to one surface of the cdb3 dimer in the vicinity of the point mutation. The results demonstrate that even subtle structural perturbations caused by point mutations in cdb3 can lead to reduced protein 4.2 binding and to the HS phenotype. Portions of this work have appeared as an abstract (*32*).

EXPERIMENTAL PROCEDURES

Cloning and Site-Directed Mutagenesis. The full-length AE1 DNA was kindly provided by Dr. Robert Gunn (Emory University). The cdb3 gene encoding residues 1−379 of AE1 was amplified using Pfu DNA polymerase (Stratagene, La Jolla, CA) with the N-terminal (forward) primer ACGGGA-ATTCCATATGGAGGAGCTGCAGGATGATTATG and the C-terminal (reverse) primer TCACACCGCTCGAGTTATT-AGAAGAGCTGGCCTGTCTGCTG (IDT DNA, Coraville, IA). The PCR product was cloned into the pET-19b vector (Novagen, Madison, WI) between the *Nde*I and *Xho*I sites, named pZZ3_WT. The cysteineless mutant (pZZ3), the cysteineless P327R mutant (pZZ4), and single-cysteine mutants were constructed using the QuikChange Site-Directed Mutagenesis Kit (Stratagene). The sequences of all mutants were confirmed by DNA sequencing.

Protein Expression, Purification, and Spin Labeling. pZZ3 and pZZ4 plasmids were transformed into BL21 Gold (DE3) *Escherichia coli* competent cells (Stratagene). Expression of cdb3 was followed by the autoinduction protocol developed by Studier (*35*). Briefly, overnight starter cultures were grown in PA-0.5G at 37 °C. Starter cultures (200 μL) were used to inoculate 200 mL of ZYP-5052 for overnight autoinduction (14 h). Typically, saturation (A_{600} = 4.8−7.0) was reached in about 10 h at 37 °C. Additional incubation for 4 h maximized lactose autoinduction. His-tagged cdb3 purification was carried out using Ni-NTA resin as described by the manufacturer (Qiagen, Valencia, CA). For some mutants, the N-terminal His tag was cleaved using the Enterokinase Cleavage Capture Kit (Novagen). Protein concentration was determined by absorption at 280 nm using an extinction coefficient of 33000 M^{-1} cm^{-1}. Protein yield was ∼8 mg per 200 mL of culture. Protein purity, as assessed by SDS-PAGE, was ≥95% for all samples studied. Single-cysteine mutants were spin-labeled with a 10-fold molar excess of MTSSL [(1-oxyl-2,2,5,5-tetramethyl-Δ3-pyrroline-3-methyl) methanethiosulfonate spin label, Toronto Research Chemicals, North York, ON, Canada] in the dark at room temperature for 2 h and then at 4 °C overnight. Unreacted spin label was removed by diluting and reconcentrating samples four times in an Amicon Ultra-4 centrifugal filter device (30K nominal molecular weight limit, Millipore, Bedford, MA) with a buffer containing 20 mM NaH_2PO_4, 100 mM NaCl, and 1 mM EDTA, pH 6.8.

Cw-EPR Measurements. X-band (9.8 GHz) cw-EPR spectra were collected on a Bruker EMX spectrometer equipped with a TM_{110} or an ER4123D resonator (Bruker Biospin, Billerica, MA) at room temperature as described in detail in previous work (*30*).

Solvent Accessibility. Solvent accessibility of individual spin-labeled residues was measured empirically on samples diluted to 100 μM spin concentration in 20 mM NaH_2PO_4, 100 mM NaCl, and 1 mM EDTA, pH 6.8. NiEDDA was added at a final concentration of 5 mM. The accessibility parameters reported provide an assessment of the steric packing of residues in the vicinity of the spin label as discussed extensively in recent work (*36*). Samples were purged of molecular oxygen by flowing nitrogen gas over the sample contained in a TPX capillary for 15 min prior to and during measurements. A 25 G scan of the central resonance line for each mutant was carried out using a 1 G modulation amplitude of 100 kHz frequency in an ER4123D dielectric resonator (Bruker Biospin). A total of 24 scans were recorded at microwave powers ranging from 1 to 200 mW (1 dB attenuation/step). Data were analyzed by nonlinear least-squares curve fitting using Origin 6.1 software (OriginLab Corp., Northampton, MA) as described in previous work (*30*). The NiEDDA accessibility was calculated by using the equation

$$\mathrm{Ac(NiEDDA)} = \frac{P_{1/2}(\mathrm{NiEDDA}) - P_{1/2}(\mathrm{N_2})}{\Delta H_0} \qquad (1)$$

where Ac is the accessibility, $P_{1/2}$ (NiEDDA) is the half-saturation power in the presence of 5 mM NiEDDA, $P_{1/2}$ (N_2) is the half-saturation power in the absence of NiEDDA, and ΔH_0 is the central line width (*37*, *38*).

DEER Measurements. Long-range nitroxide−nitroxide distances were measured by DEER spectroscopy. DEER experiments were performed at X-band using a Bruker E680 X/W-band instrument (Bruker Biospin) at the National High Magnetic Field Laboratory (Tallahassee, FL) or on an in-house Bruker E580 X-band instrument using a standard four-pulse sequence (*39*). For DEER measurements, spin-labeled cdb3 dimer samples ranged from 75 to 300 μM in spin-label concentration as measured by the doubly integrated intensity of the room temperature cw-EPR spectrum compared to a standard of known spin concentration. All samples contained 30% (w/w) glycerol. All DEER experiments were performed at 65 K using a 1 ms shot repetition time and a 16 ns 90° pulse width in an overcoupled dielectric resonator (ER 4118X-MD5, Bruker Biospin). The 180° ELDOR pulse was 32 ns wide at 70 MHz frequency offset. DEER data were analyzed using the DeerAnalysis 2006 software made available by G. Jeschke [Max Planck Institute for Polymer Research, Mainz, Germany (*40*−*42*)] assuming either a single or a double Gaussian distance distribution given by the formulas

$$P(R) = \frac{1}{\sqrt{2\pi}\sigma} e^{-(R-R_0)^2/2\sigma^2} \quad (2)$$

$$P(R) = \frac{(1-x)}{\sqrt{2\pi}\sigma_1} e^{-[R-(R_0)_1]^2/2\sigma_1^2} + \frac{x}{\sqrt{2\pi}\sigma_2} e^{-[R-(R_0)_2]^2/2\sigma_2^2} \quad (3)$$

RESULTS

Effect of the P327R Mutation on the Local Structure and Spatial Arrangement of the Peripheral Domains of Cdb3. The cdb3 dimerization domains have a high degree of homology among species with four proline residues at positions 322, 323, 327, and 337 conserved in chicken, rat, mouse, frog, dog, horse, and human erythrocyte band 3. It has been suggested that substitution of an arginine for one of these conserved prolines might result in dissociation of the cdb3 dimer (*28*, *31*). Recent data from native gel electrophoresis (*32*) and ultracentrifugation (*33*, *34*) have indicated that the P327R mutation does not alter the oligomeric state of wt cdb3, and CD has shown that there are no major changes in secondary structure (*34*). To investigate the effects of the P327R substitution on the local structure of the two peripheral domains of the cdb3 dimer and their spatial arrangement in more detail, SDSL coupled with electron paramagnetic resonance (SDSL-EPR) was employed on the cys-less-cdb3 background with the P327R mutation. A series of single-cysteine mutants were expressed, purified, and spin-labeled with MTSSL (Figure 1) to yield the spin-labeled side-chain designated R1 (*43*).

A total of 11 sites along the surface of the peripheral domains proximal to the dimer interface were chosen for initial characterization (Figure 2). The EPR signals at all 11 sites are remarkably similar between the P327 and R327 backgrounds. These results demonstrate that the P327R substitution does not significantly affect the local structure, as reflected in side-chain mobility, at any of the selected

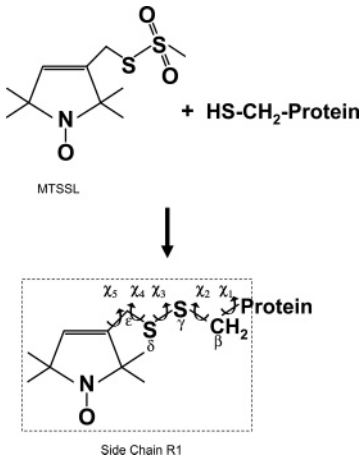

FIGURE 1: Protein labeling with MTSSL. The reaction of cysteine with MTSSL yields the spin-labeled side chain denoted R1. The dihedral angles χ_1 through χ_5, which relate the spin label moiety to the protein backbone, are defined in accordance with the previous literature (*55*).

sites on the two peripheral domains. The spectra from L108R1 show the same strong intermonomer spin−spin coupling between the R1 side chains with both the P327 and R327 backgrounds. This result demonstrates that cdb3-R327 is dimeric as reported in previous work (*34*) and that the spatial separation and relative orientation of the two interacting R1 side chains at this site are the same in both samples. Collectively, the data in Figure 2 show that the R1 side chains at 11 separate positions are in essentially indistinguishable local environments under the two backgrounds. Therefore, the structure of an extensive region of the peripheral domain does not appear to be affected by the P327R point mutation. This conclusion is supported by EPR data at additional sites in the peripheral domain as summarized in Figure 9.

On the basis of the static crystal structure of cdb3 (*29*), the intradimer distances between the R1 side chains at all positions shown in Figure 2 except for L108R1 and R112R1 are predicted to be in the 18−50 Å range and, consequently, not readily measurable by cw-EPR. Therefore, the average interprobe distances and the corresponding distance distributions at the remaining nine sites were determined by DEER as shown in Figure 3. The data from all nine sites show conclusively that cdb3 remains dimeric and that the average interprobe distances are remarkably similar between the P327 and R327 backgrounds. These results argue against any significant rearrangement in the relative spatial disposition of the two peripheral domains as a result of the P327R mutation. Even though changes in the average interprobe distances were small (<3 Å) at all sites, changes in the widths of the recovered distance distributions at some sites (e.g., 96 and 199) were observed as shown in Figure 3 (bottom panel). These observations will be considered in greater detail under Discussion.

Effect of the P327R Mutation on the Local Structure and Spatial Arrangement of the C-Terminal End of Helix 10 at the Dimer Interface of Cdb3. P327 is located in the loop (residues 324−327), which connects β-strand 11 (residues 318−323) and α-helix 10 (residues 328−347) at the dimer interface. Therefore, it is in a position that could contribute significantly to the structure and dynamics of the dimer interface. Therefore, R1 side-chain mobility and solvent

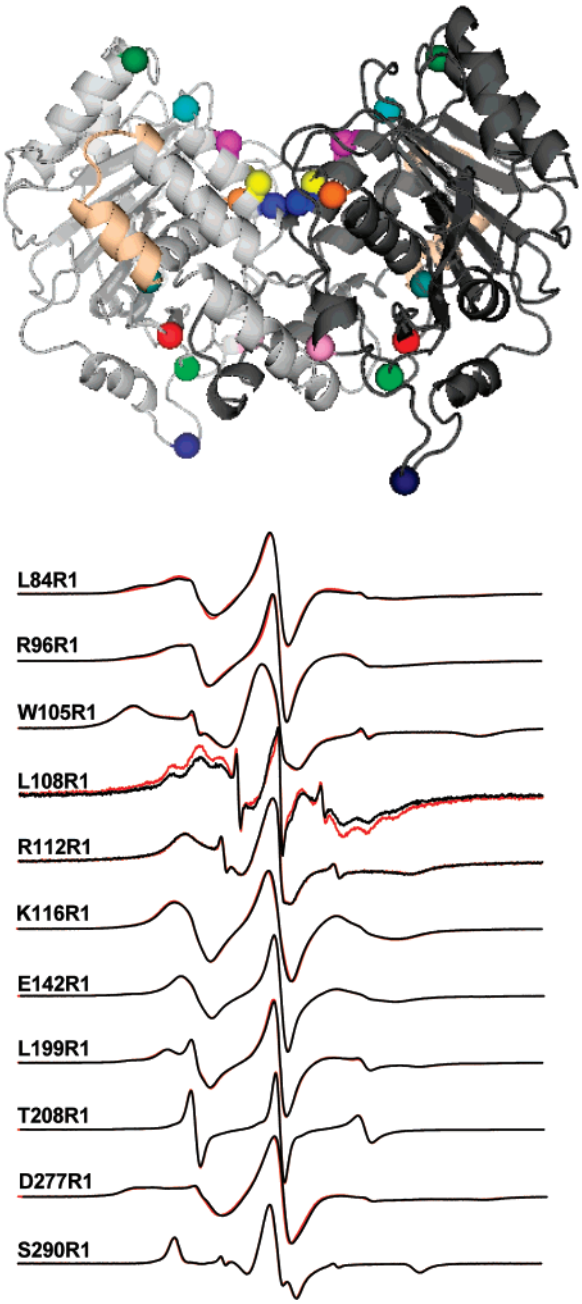

FIGURE 2: EPR line shapes of P327 and R327 forms of cdb3 at selected residues on the peripheral domains. (Top) Ribbon diagram of the cdb3 dimer. R1 side chains at positions 84 (red), 96 (green), 105 (dark blue), 108 (yellow), 112 (purple), 116 (light blue), 142 (dark green), 199 (pink), 208 (blue), 277 (orange), and 290 (medium blue) are marked as spheres on the α-carbons. (Bottom) Direct comparison of EPR line shapes obtained from P327 cdb3 (red line) and R327 mutant (black line) backgrounds. The spectra are normalized to the same amplitude for easy comparison. The spectral widths for all samples are 100 G except for L108R1, which is 200 G, and S290R1, which is 150 G.

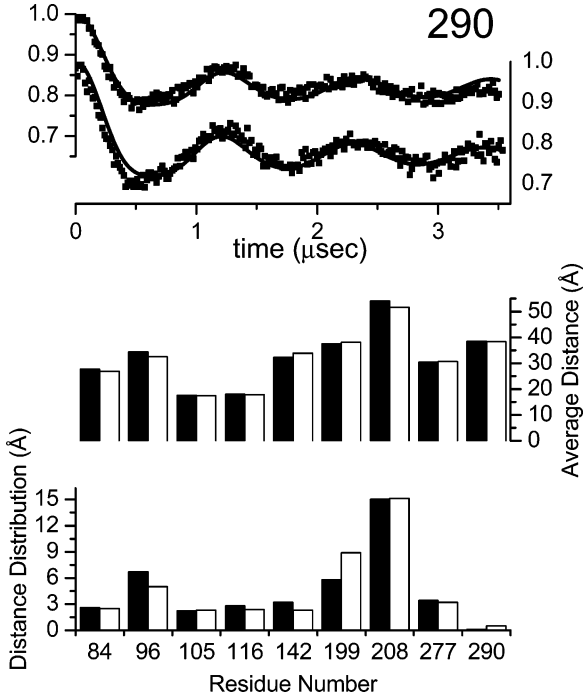

FIGURE 3: Comparison of DEER results at sites on the peripheral domains of wt P327 and variant R327 backgrounds. (Top) Experimental DEER data (dots) obtained from wt P327 (upper) and variant R327 (lower) backgrounds at residue 290. The continuous black lines in each display are the best fits to the experimental data using a single Gaussian distribution of interprobe distances. (Middle) Histogram showing average interprobe distance determined at each site for the wt P327 (black bars) and variant R327 (white bars) backgrounds using a single Gaussian distribution of distances. (Bottom) Histogram showing the widths of the corresponding distance distributions at each site.

accessibility at sites 337−348 were measured as shown in Figures 4 and 5.

The EPR spectra from sites 337−348 were almost indistinguishable in the P327 and R327 backgrounds except at 339, 340, 343, and 346 as shown in Figure 4. Interestingly, each of the sites that showed spectral changes lies on the same face of helix 10 that is packed in close proximity to helix 9 from the same monomer and to the loop region between β-strand 11 and helix 10 of the other monomer and, hence, is shielded from solvent exposure. These residues are shown as pink spheres in the structure at the top of Figure 4. The approximate 3.6 residue periodicity of side-chain mobility, as reported previously for the P327 background (*30*), is evident for the R327 background as well indicating that this section of helix 10 remains intact and that approximately the same surface of the helix makes tertiary/quaternary contacts with the underlying structural elements. The data indicate that even though there does not appear to be any measurable rigid body rotation of this portion of helix 10, there are subtle changes in the way that residues 339, 340, 343, and 346 interact with helix 9 and/or the loop of the adjacent monomer. The large spectral change observed at residue 339 is most likely due to a direct side-chain repacking effect resulting from replacing P327 with R327 rather than a displacement of the entire helix as discussed more fully below.

Figure 5 shows the parametrized data for accessibility of the R1 side chain at sites 337−348 to the water-soluble paramagnetic broadening agent NiEDDA. The data from the P327 background, shown in solid squares in Figure 5, exhibit the expected 3.6 residue periodicity in solvent accessibility for a surface-exposed α-helix. Moreover, residues 339, 342, and 346 show the lowest solvent accessibility, in excellent agreement with the packing interface of this surface-exposed helix in the crystal structure as described in previous work (*30*). The data from the R327 variant, shown as open squares in Figure 5, follow the general trend of P327 from residue 337 to 342. However, from residue 343 through 347, there

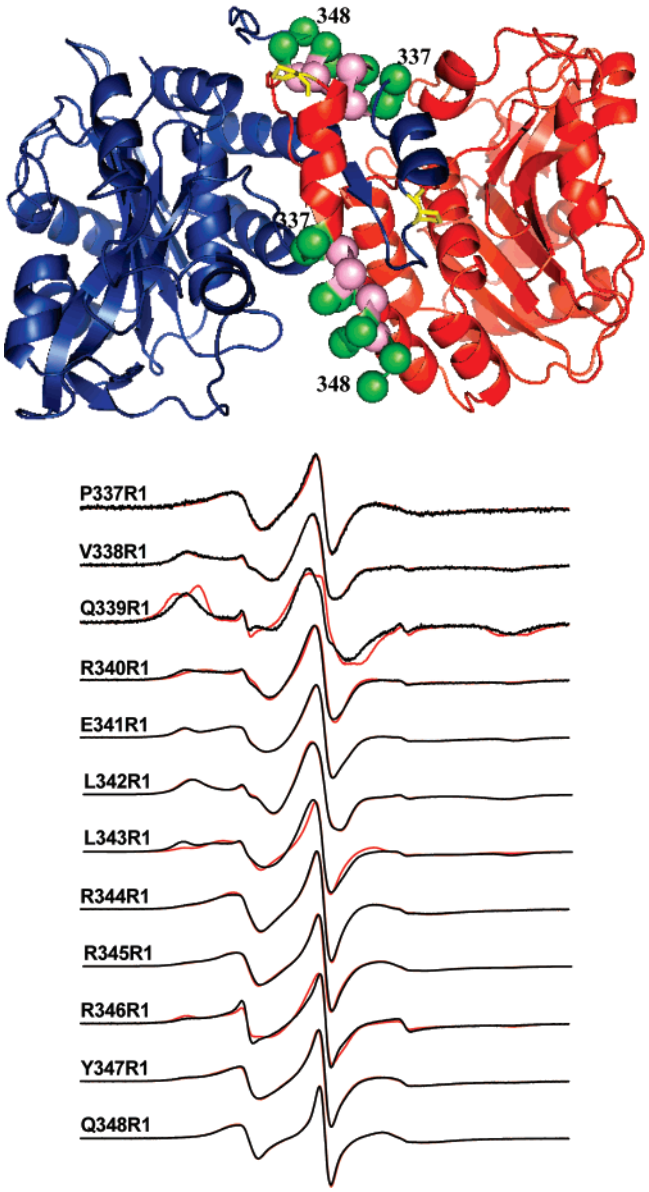

FIGURE 4: EPR line shapes of P327 and R327 forms of cdb3 at residues 337−348 on helix 10 of the dimerization arm. (Top) Ribbon diagram of the cdb3 dimer with one subunit in red and the other in blue. R1 sites at residues 339, 340, 343, and 346 where changes in the EPR spectra are observed are shown as pink spheres on the α-carbons. Other labeled sites are shown as green spheres. The side chain of P327 is shown in yellow. (Bottom) Comparison of EPR line shapes from wt P327 (red line) and variant R327 (black line) forms of cdb3. The spectra are normalized to the same amplitude for comparison. The spectral widths for each sample are 100 G.

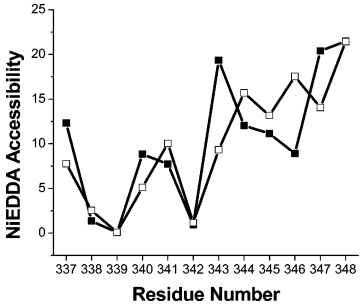

FIGURE 5: NiEDDA accessibility of the R1 side chain from sites 337−348. The filled squares are measured NiEDDA accessibilities of wt P327 cdb3 from residues 337R1 to 348R1. The open squares are the measured NiEDDA accessibilities of the P327R variant from 337R1 to 348R1.

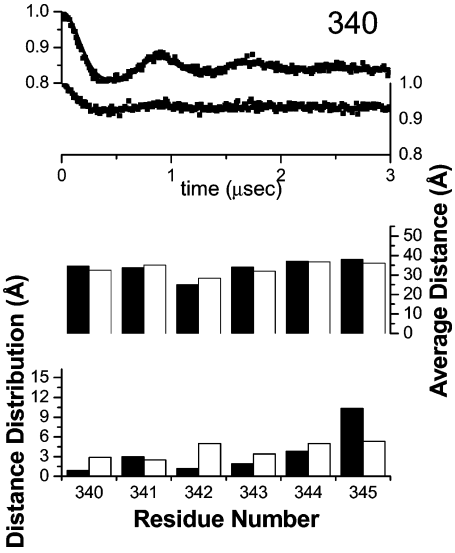

FIGURE 6: Comparison of DEER results at sites 340−345 on helix 10 of the dimerization arms with wt P327 and variant R327 backgrounds. (Top) Experimental DEER data (dots) obtained from wt P327 (upper) and variant R327 (lower) backgrounds at residue 340. The continuous black lines in each display are the best fits to the experimental data using a single Gaussian distribution of interprobe distances. (Middle) Histogram showing the average interprobe distance determined at each site for the wt P327 (black bars) and variant R327 (white bars) backgrounds using a single Gaussian distribution of distances. (Bottom) Histogram showing the widths of the corresponding distance distributions at each site.

are noticeable differences in solvent accessibility, particularly at residues 343, 346, and 347. It is interesting to note that the EPR data in Figure 4 showed changes in side-chain dynamics at residues 343 and 346. At residue 343, the P327R mutation resulted in the enhancement of a highly immobilized component in the spectrum, indicative of increased tertiary/quaternary contact. Conversely, at residue 346, the P327R mutation resulted in reduction of a highly immobilized component, indicative of decreased tertiary/quaternary contact at this site. These observations agree with the differences in solvent accessibility determined at these sites. The data in Figures 4 and 5 suggest that there are subtle changes in the packing and interactions of the C-terminal end of helix 10 in the R327 variant. These observations alone do not provide any insight into whether the local structure of all dimers in the ensemble is affected or whether the observed changes are due to generation of a heterogeneous structural distribution.

To further characterize structural changes resulting from the P327R mutation, DEER experiments were carried out to measure the intermonomer nitroxide−nitroxide distances between residues 340−345 as shown in Figure 6. At all six sites the average interprobe distances for the P327 and R327 backgrounds, which were determined by fitting the experimental data to a single Gaussian distribution, agreed to within 0.3−3.4 Å. There are no systematic changes in interprobe distances indicative of rotation or translation of the entire helix. These results support the conclusion that the P327R mutation does not lead to any large-scale alterations in the apparent relative spatial orientation of the two helices in the cdb3 dimer. However, at sites 340, 342,

Table 1: Comparison of Single and Double Gaussian Distance Distribution Analyses of DEER Data for Residues 340−345 in the Wild Type (wt) P327 and Variant R327 Proteins[a]

		one site			two site					
residue	protein	R_0 (Å)	σ (Å)	χ^2	$(R_0)_1$ (Å)	σ_1 (Å)	$(R_0)_2$ (Å)	σ_2 (Å)	x	χ^2
340	wt	34.6	0.9	5.4	34.7	1.1	29.8	2.1	0.87	5.2
	variant	32.6	3.1	4.6	34.5	1.1	26.7	4.1	0.39	4.4
341	wt	30.4	4.4	4.7	34.9	1.2	26.3	4.6	0.60	4.2
	variant	35.2	2.7	3.5	35.9	1.7	34.0	4.4	0.49	3.5
342	wt	24.3	1.2	1.7	24.3	1.2	78.8	4.8	0.01	1.7
	variant	25.9	3.9	2.3	24.9	1.7	31.1	9.7	0.33	2.1
343	wt	34.1	2.1	3.1	32.5	1.3	35.5	1.3	0.47	3.1
	variant	32.3	3.8	3.2	34.9	2.1	28.8	3.6	0.48	3.1
344	wt	37.6	4.6	3.7	33.0	1.1	39.2	3.6	0.25	3.7
	variant	37.1	5.5	4.2	38.9	3.7	18.7	0.4	0.19	3.8
345	wt	36.6	9.1	7.8	15.0	0.4	38.0	7.9	0.87	7.5
	variant	36.7	6.9	5.4	36.0	5.0	62.0	0.4	0.13	4.5

[a] Fit parameters are defined in eqs 2 and 3. The χ^2 values give the sum of the squared residuals of the fits versus the data.

343, and 345, the P327R mutation resulted in a change in the width of the recovered distance distributions by a factor of ≥1.3.

The DEER data from sites 340−345 were reanalyzed using a bimodal Gaussian distribution of distances as summarized in Table 1. As shown in Figure 7, the data from site 342 on the P327 background led to the recovery of a single major population with the same average interprobe distance and distance distribution that were recovered using a single Gaussian distribution of distances. With the R327 variant, the bimodal fit to the DEER data at site 342 was visibly better than that to the single-site model as indicated by the residuals in Figure 7. Moreover, the bimodal fit indicated the existence of a second component of approximately 30% of the total integrated amplitude, which exhibited a longer average interprobe distance and a much broader distribution of distances. This same level of structural heterogeneity was identified when the DEER data were reanalyzed using the model-independent Tikhonov regularization approach (data not shown). Similar results were obtained at sites 340 and 343 as summarized in Table 1. At sites 340, 342, and 343, between 52 and 67% of the total integrated signal amplitude was described by the same average interprobe distance and distribution of distances that were observed in the P327 background. Refitting of the DEER data for wt and P327R at sites 341, 344, and 345 using a bimodal distribution of distances did not result in a visibly better fit of the data compared to a single Gaussian distribution. This is not unexpected given the very broad distribution of distances observed at these sites and, hence, a relatively featureless echo amplitude modulation pattern. These observations suggest that the P327R mutation alters the dimer interface sufficiently to allow a subpopulation of helix 10 to adopt an altered packing arrangement.

Effect of the P327R Mutation on Residues in Helix 9, β-Strand 11, and the N-Terminal End of Helix 10 of Cdb3. The dimerization arms include α-helix 9 (304−316), *β*-strand 11 (318−323), α-helix 10 (328−347), and residues connecting these secondary structure elements in each subunit (*29*). From the crystal structure of wt cdb3, two major interactions at the dimer interface exist. Two *β*-strands 11 (318−323), one from each monomer, form an antiparallel

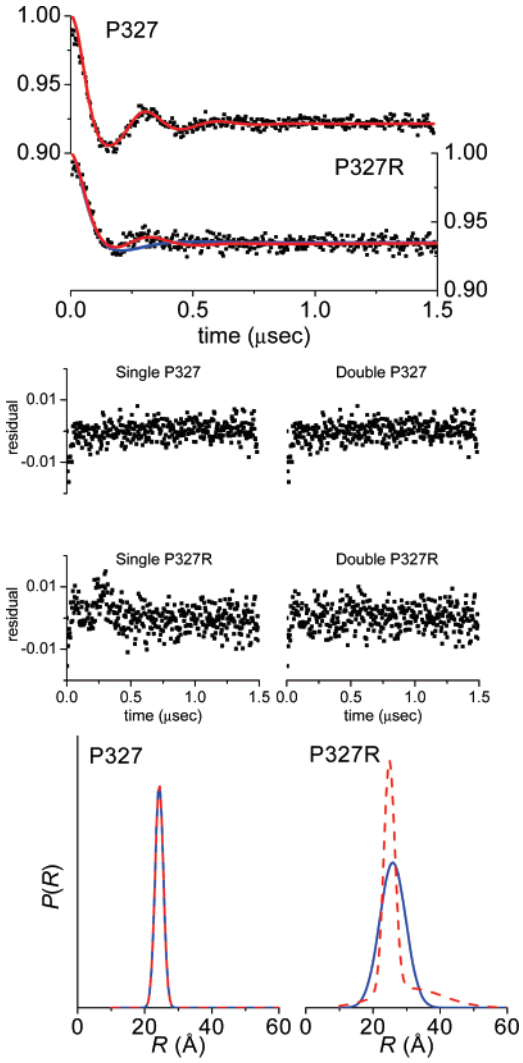

FIGURE 7: Analysis of DEER data at residue 342 of the dimerization arm. (Top) Experimental DEER data (dots) obtained from wt P327 (upper) and variant R327 (lower) backgrounds at residue 342. The continuous blue and the red lines superimposed on the experimental data are the best fits using a single Gaussian and a double Gaussian distribution of interprobe distances, respectively. (Middle) Residuals of the fits using a single Gaussian distribution of distances (left column) and a double Gaussian distribution of distances (right column). (Bottom) Recovered distribution of distances using a single Gaussian (blue solid line) or a double Gaussian (red dotted line) model for wt P327 (lower left) and variant R327 (lower right) cdb3.

β-sheet, which contributes 8 intermonomeric backbone-to-backbone hydrogen bonds. A hydrophobic core of 9 interacting leucine residues (from α-helices 10, *β*-strands 11) also stabilizes the dimer configuration (*29*). To determine if the P327R mutation disrupts these critical interactions, residues 312 and 313 at the C-terminal end of helix 9, residue 321 on *β*-strand 11, and residues 329, 332, and 333 on the N-terminal end of helix 10 were separately converted to the R1 side chain and their EPR spectra characterized as shown in Figure 8. At positions 312 and 313, the data from the P327 and R327 backgrounds were identical. At L321R1, the major spectral component on both P327 and R327 backgrounds is severely broadened due to spin−spin interactions (<10 Å) between the two nitroxides at the dimer interface. However, there is a second minor component with the R327 variant, marked by the arrows in Figure 8, that exhibits a splitting of almost 200 G indicative of very strong spin−

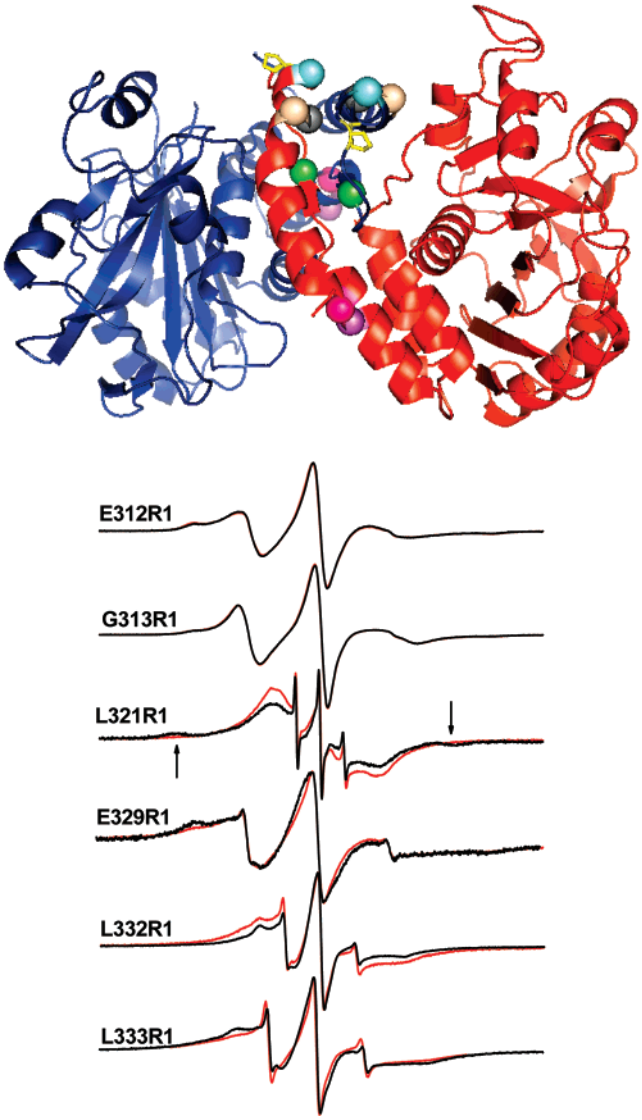

FIGURE 8: EPR spectra of wt P327 and variant R327 cdb3 at selected sites in the dimerization arms. (Top) Ribbon structure of the cdb3 dimer with the selected R1 sites highlighted as spheres on the α-carbons: 312 (magenta), 313 (pink), 321 (green), 329 (cyan), 332 (gray), and 333 (tan). The P327 side chain is shown in yellow. The bottom panel shows EPR line shapes from wt P327 (red line) and variant R327 (black line) cdb3. The spectra are normalized to the same amplitude for easy comparison. The spectral widths for sites E312R1, G313R1, and E329R1 are 100 G, the spectral widths for E332R1 and L333R1 are 200 G, and the spectral width for E321R1 is 300 G. The black arrows indicate a new spectral component observed for the R327 variant at residue 321.

spin interactions in a subpopulation of cdb3. The EPR data at positions 329R1, 332R1, and 333R1, on both backgrounds, show the same spectral components but with slightly different relative intensities. These observations provide direct evidence that the P327R mutation does not cause major disruption of important backbone-to-backbone hydrogen bonds and hydrophobic interactions at the dimer interface. Subtle EPR line shape changes between the P327 and R327 proteins were detected at sites 321R1, 329R1, 332R1, and 333R1. From the crystal structure of wt cdb3, Cα−Cα distances between P327 and E312, G313, L321, E329, L332, and L333 within one subunit are approximately 32, 30, 13, 6, 9, and 10 Å, respectively. The α-carbons of E312 and G313 are closer to the α-carbon of P327 from another monomer with distances of 24 and 21 Å. These data suggest that the perturbation of making the P327R mutation is localized to residues close to site 327 (a radius of ∼10−12 Å) in the dimerization arm.

DISCUSSION

Clinically, the P327R mutation leads to an HS phenotype with moderate hemolytic anemia. Erythrocyte membranes show normal levels of AE1, normal ankyrin binding, and a 29% reduction in the content of protein 4.2 (*28*), suggesting that this point mutation may produce the HS phenotype by altering the binding affinity of protein 4.2 via changes in the structure of cdb3. Previous work by Bustos and Reithmeier (*34*) showed that the P327R mutation did not dissociate the cdb3 dimer, that the overall secondary structure, as reported by CD, was unaltered, and that the urea denaturation profile was also unaltered. However, there was a modest reduction in thermal stability with the P327R variant exhibiting a 5° decrease in melting temperature in agreement with the work of Zhou et al. (*32*). Whereas these previous studies showed conclusively that the P327R mutation did not produce large changes in the overall structure of the cdb3 dimer, they did not have the resolution to probe which regions of the protein were affected by the point mutation.

Site-directed spin labeling has emerged as a powerful technique for probing the structural consequences of various perturbations including disease-causing point mutations as discussed in recent reviews (*44*−*46*). SDSL is particularly powerful when a static crystal structure has been solved, and therefore logical choices can be made regarding where to incorporate R1 side chains in order to probe specific structural features. In the current studies, SDSL has been utilized, in conjunction with the crystal structure of wt-cdb3 (*29*), to incorporate R1 side chains at specific positions in order to address two overriding questions. First, does the P327R mutation cause any significant change in the global structure of cdb3 as reflected in the peripheral domains or in their relative orientation? Second, does the P327R mutation affect the structure and spatial arrangement of residues near the mutation site in the dimerization arms of the cdb3 dimer?

The proline side chain is unique among the naturally occurring amino acids. It is often observed to be a helix breaker (*47*) due to the rotational restriction of the N−Cα bond, the steric effect of the pyrroline ring, and the lack of an amide NH hydrogen bond donor. Proline also has a high propensity as a helix-capping residue (*48*) as well as a connecting residue in *β*-turns and in loop regions (*49*, *50*). Given the positioning of P327 as the N-terminal cap for α-helix 10 and its location at the end of the loop that connects *β*-strand 11 and α-helix 10 at the dimer interface of cdb3, the P327R point mutation potentially could result in significant structural changes as discussed in previous work by Low and co-workers (*29*). One type of structural change that is possible without any change in secondary or quaternary structure is a twisting or rotation of the two peripheral domains relative to the dimer interface. To test this possibility, 11 separate sites along the surface of the peripheral domain that is proximal to the pseudo C_2 axis were chosen for incorporation of the R1 side chain as shown in Figure 2.

The EPR line shapes at all 11 sites were almost identical between the P327 and R327 backgrounds. This shows that the secondary and tertiary structures, as reported by R1 side-chain dynamics, are not significantly altered by the P327R mutation. The DEER data in Figure 3 indicate that the mutation also does not dramatically affect the quaternary structure of the cdb3 dimer because the average interprobe distances at all sites were remarkably similar. Any rigid body twisting or rotation of the two peripheral domains would lead to systematic changes in interprobe distances that would be easily recognizable. Interestingly, subtle changes in the widths of the distance distributions were observed at some residues, including 96 and 199 as shown in Figure 3, although the average distances are virtually identical. These sites are both close, in three-dimensional space, to the site of the point mutation, suggesting that the structural changes are highly localized.

To further identify the structural changes, residues 337−348 in helix 10 were individually converted to the R1 side chain and the EPR spectra characterized. The data in Figure 4 show that all of the sites that are surface exposed give identical EPR spectra in the two backgrounds. All sites that are buried or at tertiary/quaternary contacts remain highly constrained with regard to side-chain dynamics, but the EPR spectra are altered at residues 340, 343, and 346 as a result of the point mutation. The periodicity observed in the data with every third to fourth residue highly constrained by packing interactions indicates that the helix remains intact and that there is no detectable rigid body rotation of the helix. Taken at face value, the data at residue 339 suggest that there could be an 8 Å lateral displacement of helix 10. Specifically, analysis of the data in the P327 background using a tether-in-a-cone model (*51*) indicated an interprobe distance of 14.7 Å (*30*), whereas analysis of the data in the variant R327 background using a convolution approach (*52*) indicated an interprobe distance on the order of 23 Å. Because none of the residues from 340 to 345 in Figure 6 indicates a similar helix displacement, the data at residue 339 most likely arise from a repacking of the R1 side chain in the R327 variant. This interpretation is supported by inspection of the static crystal structure, where it is seen that the side chain of residue 327 is very close to the modeled R1 side chain at position 339. Therefore, the nonconservative substitution of the charged arginine residue for proline at position 327 could favor an alternate packing arrangement for the R1 side chain at residue 339. It is also possible that this point mutation could favor repacking of the native glutamine residue at position 339, although these studies cannot readily address this possibility.

When the DEER data from residues 340−345 in Figure 6 were initially analyzed in terms of a single Gaussian distribution of distances, it appeared that the major effect of the P327R mutation was a broadening of the distance distributions at residues 340, 342, 343, and 344 and an apparent narrowing of the very broad distance distribution at residue 345 with only minimal changes in the average interprobe distances (Table 1). However, when the data were reanalyzed using a double Gaussian distribution of distances (Table 1) or by Tikhonov regularization (data not shown), it was observed that at some sites, including residues 340, 342 (Figure 7), and 343, the fits to the data were visually improved as compared to a single Gaussian distribution of distances. This is readily appreciated by inspection of the residuals to the fits at residue 342 in Figure 7, where the single Gaussian distribution misses important oscillations in the modulation pattern of the echo amplitude. The same pattern of residuals was observed for the single and double Gaussian fits at residues 340 and 343 (data not shown).

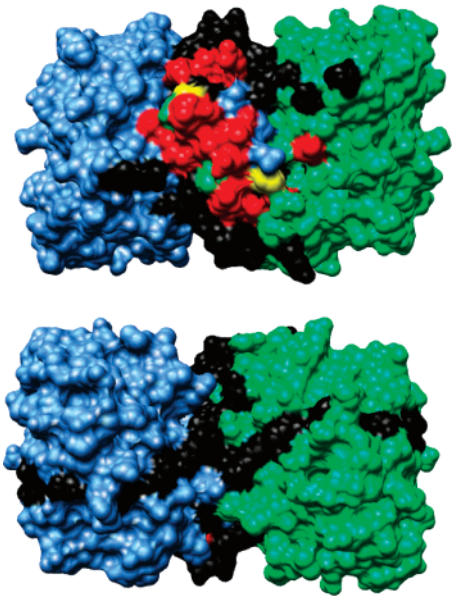

FIGURE 9: Mapping the sites of EPR spectral changes onto the crystal structure of cdb3. The red and black residues highlight the sites that were characterized by SDSL including the 11 residues shown in Figure 2, the 12 residues shown in Figure 4, and the 6 residues shown in Figure 8. Data are also included for residues 127−130, 132, 133, 135−137, 195, 293, 294, 304, 308, 314, 317, 319, 324−326, 328, 330, 352, and 355. Red residues showed spectral changes (i.e., changes in side-chain mobility, side-chain accessibility, and/or widths of interprobe distance distributions) as a result of the P327 mutation. Black residues showed no spectral changes. P327 is shown in yellow. The two views of the cdb3 dimer are along the pseudo C_2 axis rotated by 180°.

The solvent accessibility data in Figure 5 indicate that the C-terminal end of helix 10 is packed differently in the R327 variant. This change in solvent accessibility could have arisen from a repositioning of the helix in all members of cdb3 in the ensemble. Alternatively, the point mutation could have resulted in repositioning of the helices in only a subpopulation of the ensemble. The DEER data at positions 340, 342, and 343 suggest that the latter explanation is likely to be correct. Because the DEER data are recorded at 60 K, different structures present in solution should be trapped in the frozen state. The DEER data indicate that a second minor population is produced by the point mutation. It should be emphasized that the cw-power saturation methods employed to measure solvent accessibility in this work do not have the capability to detect multiple structural species with different accessibilities. Instead, the values determined are average accessibilities for all species present. Further tests of the validity of the two population model predicted from the DEER data will require more sophisticated methods for measuring solvent accessibility such as pulsed saturation recovery where the T_{1e} values for all species present are measured directly (*53*). The important overall point to be made with regard to the current study is that the data in Figures 5−7 indicate that the P327R mutation leads to greater

heterogeneity in the positioning of the C-terminal end of helix 10.

The data in Figure 8 demonstrate that the P327R mutation also slightly perturbs the structure of the N-terminal end of helix 10 as shown by the observed changes in side-chain dynamics at sites 329, 332, and 333 as well as the packing of β-strands 11 as shown by the appearance of a new spectral component due to interprobe dipolar interactions at site 321. However, the perturbation does not appear to extend to the C-terminal end of helix 9 because the EPR data at sites 312 and 313 were identical. This interpretation is also supported by interprobe distance measurements at site 312, where the average interprobe distance and distribution of distances was the same in both backgrounds (data not shown). Molecular dynamics simulations are in progress to examine the effects of the P327R mutation on the packing of cdb3 in greater detail.

Figure 9 shows a compilation of the data presented in Figures 2−8 mapped onto the static crystal structure of the cdb3 dimer. The sites where R1 side chains were incorporated into cdb3 in both the wt P327 protein and the R327 variant and where no spectral changes were observed are shown in black. Sites where changes in side-chain dynamics, in solvent accessibility, or in interprobe distance distributions were observed are shown in red. This mapping shows that there is a surface on one face of the dimer that is affected by the point mutation, whereas the opposite face is virtually unaffected. Given that previous studies have shown that cdb3 is the primary binding site for protein 4.2 (*54*) and that the P327R mutation leads to a reduction in the amount of protein 4.2 in the membrane (*28*), it is reasonable to hypothesize that the red surface of the cdb3 dimer shown in the upper panel of Figure 9 is involved in the protein−protein interaction with protein 4.2. The spin-labeled constructs developed in this work can be used to directly test this hypothesis in future work.

In conclusion, the P327R mutation in AE1 results in a subtle change in the local structure of the cdb3 dimer near the mutation site. No changes were detected in the structures of the distal portions of the peripheral domains or in the relative positioning of the peripheral domains relative to the dimer interface. Even though residues in β-strand 11 and α-helix 10, which flank the mutation site, showed measurable spectral changes, it does not appear that changes in secondary structure occur or that the elements of secondary structure are displaced. Instead, it appears that the point mutation causes some heterogeneity in the local structure of the dimer interface, possibly involving an altered packing of the C-terminal end of helix 10 in a subpopulation of the ensemble. The studies show that the spectral changes map to a specific surface of the cdb3 dimer, thereby potentially providing insight into one binding site for protein 4.2.

ACKNOWLEDGMENT

We thank Dr. Hassane Mchaourab (Vanderbilt) for critiquing the manuscript prior to submission and for many helpful discussions during the course of the work. We gratefully acknowledge Drs. Piotr Fajer and Jurek Krzystek (both from the National High Magnetic Field Laboratory, Tallahassee, FL) for providing assistance in obtaining initial DEER data presented here.

REFERENCES

1. Skalak, R., and Branemark, P. I. (1969) Deformation of red blood cells in capillaries, *Science 164*, 717−719.
2. Tanner, M. J. (2002) Band 3 anion exchanger and its involvement in erythrocyte and kidney disorders, *Curr. Opin. Hematol. 9*, 133−139.
3. Tse, W. T., Lecomte, M. C., Costa, F. F., Garbarz, M., Feo, C., Boivin, P., Dhermy, D., and Forget, B. G. (1990) Point mutation in the β-spectrin gene associated with α I/74 hereditary elliptocytosis. Implications for the mechanism of spectrin dimer self-association, *J. Clin. Invest. 86*, 909−916.
4. Feo, C. J., Fischer, S., Piau, J. P., Grange, M. J., and Tchernia, G. (1980) First instance of the absence of an erythrocyte membrane protein (band 4(1)) in a case of familial elliptocytic anemia, *Nouv. Rev. Fr. Hematol. 22*, 315−325.
5. Tchernia, G., Mohandas, N., and Shohet, S. B. (1981) Deficiency of skeletal membrane protein band 4.1 in homozygous hereditary elliptocytosis. Implications for erythrocyte membrane stability, *J. Clin. Invest. 68*, 454−460.
6. Conboy, J., Mohandas, N., Tchernia, G., and Kan, Y. W. (1986) Molecular basis of hereditary elliptocytosis due to protein 4.1 deficiency, *N. Engl. J. Med. 315*, 680−685.
7. Gallagher, P. G., and Ferriera, J. D. (1997) Molecular basis of erythrocyte membrane disorders, *Curr. Opin. Hematol. 4*, 128−135.
8. Delaunay, J. (2002) Molecular basis of red cell membrane disorders, *Acta Haematol. 108*, 210−218.
9. Bennett, V., and Baines, A. J. (2001) Spectrin and ankyrin-based pathways: metazoan inventions for integrating cells into tissues, *Physiol. Rev. 81*, 1353−1392.
10. Birkenmeier, C. S., and Barker, J. E. (2004) Hereditary haemolytic anaemias: unexpected sequelae of mutations in the genes for erythroid membrane skeletal proteins, *J. Pathol. 204*, 450−459.
11. Tanner, M. J. (1997) The structure and function of band 3 (AE1): recent developments (review), *Mol. Membr. Biol. 14*, 155−165.
12. Fairbanks, G., Steck, T. L., and Wallach, D. F. (1971) Electrophoretic analysis of the major polypeptides of the human erythrocyte membrane, *Biochemistry 10*, 2606−2617.
13. Steck, T. L., Ramos, B., and Strapazon, E. (1976) Proteolytic dissection of band 3, the predominant transmembrane polypeptide of the human erythrocyte membrane, *Biochemistry 15*, 1153−1161.
14. Tanner, M. J., Martin, P. G., and High, S. (1988) The complete amino acid sequence of the human erythrocyte membrane anion-transport protein deduced from the cDNA sequence, *Biochem. J. 256*, 703−712.
15. Lux, S. E., John, K. M., Kopito, R. R., and Lodish, H. F. (1989) Cloning and characterization of band 3, the human erythrocyte anion-exchange protein (AE1), *Proc. Natl. Acad. Sci. U.S.A. 86*, 9089−9093.
16. Lepke, S., and Passow, H. (1976) Effects of incorporated trypsin on anion exchange and membrane proteins in human red blood cell ghosts, *Biochim. Biophys. Acta 455*, 353−370.
17. Grinstein, S., Ship, S., and Rothstein, A. (1978) Anion transport in relation to proteolytic dissection of band 3 protein, *Biochim. Biophys. Acta 507*, 294−304.
18. Low, P. S. (1986) Structure and function of the cytoplasmic domain of band 3: center of erythrocyte membrane−peripheral protein interactions, *Biochim. Biophys. Acta 864*, 145−167.
19. Bennett, V., and Stenbuck, P. J. (1980) Association between ankyrin and the cytoplasmic domain of band 3 isolated from the human erythrocyte membrane, *J. Biol. Chem. 255*, 6424−6432.
20. Rybicki, A. C., Schwartz, R. S., Hustedt, E. J., and Cobb, C. E. (1996) Increased rotational mobility and extractability of band 3 from protein 4.2-deficient erythrocyte membranes: evidence of a role for protein 4.2 in strengthening the band 3-cytoskeleton linkage, *Blood 88*, 2745−2753.
21. Pasternack, G. R., Anderson, R. A., Leto, T. L., and Marchesi, V. T. (1985) Interactions between protein 4.1 and band 3. An alternative binding site for an element of the membrane skeleton, *J. Biol. Chem. 260*, 3676−3683.
22. Low, P. S., Willardson, B. M., Mohandas, N., Rossi, M., and Shohet, S. (1991) Contribution of the band 3-ankyrin interaction to erythrocyte membrane mechanical stability, *Blood 77*, 1581−1586.
23. Peters, L. L., Shivdasani, R. A., Liu, S. C., Hanspal, M., John, K. M., Gonzalez, J. M., Brugnara, C., Gwynn, B., Mohandas, N., Alper, S. L., Orkin, S. H., and Lux, S. E. (1996) Anion exchanger

1 (band 3) is required to prevent erythrocyte membrane surface loss but not to form the membrane skeleton, *Cell 86*, 917−927.
24. Southgate, C. D., Chishti, A. H., Mitchell, B., Yi, S. J., and Palek, J. (1996) Targeted disruption of the murine erythroid band 3 gene results in spherocytosis and severe haemolytic anaemia despite a normal membrane skeleton, *Nat. Genet. 14*, 227−230.
25. Moriyama, R., Ideguchi, H., Lombardo, C. R., Van Dort, H. M., and Low, P. S. (1992) Structural and functional characterization of band 3 from Southeast Asian ovalocytes, *J. Biol. Chem. 267*, 25792−25797.
26. Schofield, A. E., Tanner, M. J., Pinder, J. C., Clough, B., Bayley, P. M., Nash, G. B., Dluzewski, A. R., Reardon, D. M., Cox, T. M., and Wilson, R. J. (1992) Basis of unique red cell membrane properties in hereditary ovalocytosis, *J. Mol. Biol. 223*, 949−958.
27. Gallagher, P. G., and Forget, B. G. (1997) Hematologically important mutations: band 3 and protein 4.2 variants in hereditary spherocytosis, *Blood Cells Mol. Dis. 23*, 417−421.
28. Jarolim, P., Palek, J., Rubin, H. L., Prchal, J. T., Korsgren, C., and Cohen, C. M. (1992) Band 3 Tuscaloosa: Pro327−Arg327 substitution in the cytoplasmic domain of erythrocyte band 3 protein associated with spherocytic hemolytic anemia and partial deficiency of protein 4.2, *Blood 80*, 523−529.
29. Zhang, D., Kiyatkin, A., Bolin, J. T., and Low, P. S. (2000) Crystallographic structure and functional interpretation of the cytoplasmic domain of erythrocyte membrane band 3, *Blood 96*, 2925−2933.
30. Zhou, Z., DeSensi, S. C., Stein, R. A., Brandon, S., Dixit, M., McArdle, E. J., Warren, E. M., Kroh, H. K., Song, L., Cobb, C. E., Hustedt, E. J., and Beth, A. H. (2005) Solution structure of the cytoplasmic domain of erythrocyte membrane band 3 determined by site-directed spin labeling, *Biochemistry 44*, 15115−15128.
31. Low, P. S., Zhang, D., and Bolin, J. T. (2001) Localization of mutations leading to altered cell shape and anion transport in the crystal structure of the cytoplasmic domain of band 3, *Blood Cells Mol. Dis. 27*, 81−84.
32. Zhou, Z., Desensi, S., Brandon, S., Dixit, N., Cobb, C. E., Hustedt, E. J., and Beth, A. H. (2005) Solution structure of cdb3 from site directed spin labeling studies and double electron−electron resonance, *Biophys. J. 88*, 265a (abstract).
33. Bustos, S. P., and Reithmeier, R. A. (2005) Molecular characterization of hereditary spherocytosis mutants in the cytosolic domain of the erythrocyte Cl-/HCO3-anion exchanger, *Biophys. J. 88*, 224a (abstract).
34. Bustos, S. P., and Reithmeier, R. A. (2006) Structure and stability of hereditary spherocytosis mutants of the cytosolic domain of the erythrocyte anion exchanger 1 protein, *Biochemistry 45*, 1026−1034.
35. Studier, F. W. (2005) Protein production by auto-induction in high-density shaking cultures, *Protein Expr. Purif. 41*, 207−234.
36. Altenbach, C., Froncisz, W., Hemker, R., McHaourab, H., and Hubbell, W. L. (2005) Accessibility of nitroxide side chains: absolute Heisenberg exchange rates from power saturation EPR, *Biophys. J. 89*, 2103−2112.
37. Subczynski, W. K., and Hyde, J. S. (1981) The diffusion−concentration product of oxygen in lipid bilayers using the spin-label T1 method, *Biochim. Biophys. Acta 643*, 283−291.
38. Altenbach, C., Flitsch, S. L., Khorana, H. G., and Hubbell, W. L. (1989) Structural studies on transmembrane proteins. 2. Spin labeling of bacteriorhodopsin mutants at unique cysteines, *Biochemistry 28*, 7806−7812.
39. Pannier, M., Veit, S., Godt, A., Jeschke, G., and Spiess, H. W. (2000) Dead-time free measurement of dipole−dipole interactions between electron spins, *J. Magn. Reson. 142*, 331−340.
40. Jeschke, G. (2002) Determination of the nanostructure of polymer materials by electron paramagnetic resonance spectroscopy, *Macromol. Rapid Commun. 23*, 227−246.
41. Jeschke, G. (2002) Distance measurements in the nanometer range by pulse EPR, *ChemPhysChem 3*, 927−932.
42. Jeschke, G., Koch, A., Jonas, U., and Godt, A. (2002) Direct conversion of EPR dipolar time evolution data to distance distributions, *J. Magn. Reson. 155*, 72−82.
43. McHaourab, H. S., Lietzow, M. A., Hideg, K., and Hubbell, W. L. (1996) Motion of spin-labeled side chains in T4 lysozyme. Correlation with protein structure and dynamics, *Biochemistry 35*, 7692−7704.
44. Columbus, L., and Hubbell, W. L. (2002) A new spin on protein dynamics, *Trends Biochem. Sci. 27*, 288−295.
45. Feix, J. B., and Klug, C. S. (1998) Site-directed spin labeling of membrane proteins and membrane interactions, *Biological Magnetic Resonance*, pp 251−281, Plenum Press, New York.
46. Hubbell, W. L., Cafiso, D. S., and Altenbach, C. (2000) Identifying conformational changes with site-directed spin labeling, *Nat. Struct. Biol. 7*, 735−739.
47. Richardson, J. S. (1981) The anatomy and taxonomy of protein structure, *Adv. Protein Chem. 34*, 167−339.
48. Aurora, R., and Rose, G. D. (1998) Helix capping, *Protein Sci. 7*, 21−38.
49. Gellman, S. H. (1998) Minimal model systems for β sheet secondary structure in proteins, *Curr. Opin. Chem. Biol. 2*, 717−725.
50. Crespo, M. D., Platt, G. W., Bofill, R., and Searle, M. S. (2004) Context-dependent effects of proline residues on the stability and folding pathway of ubiquitin, *Eur. J. Biochem. 271*, 4474−4484.
51. Hustedt, E. J., Stein, R. A., Sethaphong, L., Brandon, S., Zhou, Z., and Desensi, S. C. (2006) Dipolar coupling between nitroxide spin labels: the development and application of a tether-in-a-cone model, *Biophys. J. 90*, 340−356.
52. Rabenstein, M. D., and Shin, Y. K. (1995) Determination of the distance between two spin labels attached to a macromolecule, *Proc. Natl. Acad. Sci. U.S.A. 92*, 8239−8243.
53. Pyka, J., Ilnicki, J., Altenbach, C., Hubbell, W. L., and Froncisz, W. (2005) Accessibility and dynamics of nitroxide side chains in T4 lysozyme measured by saturation recovery EPR, *Biophys. J. 89*, 2059−2068.
54. Korsgren, C., and Cohen, C. M. (1988) Associations of human erythrocyte band 4.2. Binding to ankyrin and to the cytoplasmic domain of band 3, *J. Biol. Chem. 263*, 10212−10218.
55. Langen, R., Oh, K. J., Cascio, D., and Hubbell, W. L. (2000) Crystal structures of spin labeled T4 lysozyme mutants: implications for the interpretation of EPR spectra in terms of structure, *Biochemistry 39*, 8396−8405.

BI700948P